

# Dynamical instabilities of Bose-Einstein condensates at the band edge in one-dimensional optical lattices

Andrew J. Ferris and Matthew J. Davis

*ARC Centre of Excellence for Quantum-Atom Optics, School of Physical Sciences, University of Queensland, Brisbane QLD 4072, Australia*

Reece W. Geursen, P. Blair Blakie, and Andrew C. Wilson

*Jack Dodd Centre for Photonics and Ultra-Cold Atoms, Department of Physics, University of Otago, P.O. Box 56, Dunedin, New Zealand*

(Received 19 June 2007; revised manuscript received 24 October 2007; published 18 January 2008)

We present a joint theoretical and experimental study of the dynamical instability of a Bose—Einstein condensate at the band edge of a one-dimensional optical lattice. The instability manifests as rapid depletion of the condensate and conversion to a thermal cloud. We consider the collisional processes that can occur in such a system, and undertake a thorough theoretical study of the dynamical instability in systems of different dimensionality. We find spontaneous scattering is an important part of this process, and thus the Gross-Pitaevskii equation is unable to accurately predict the dynamics in this system. Our beyond mean-field approach, known as the truncated Wigner method, allows us to make quantitative predictions for the processes of parametric growth and heating that are observed in the laboratory, and we find good agreement with the experimental results.

DOI: [10.1103/PhysRevA.77.012712](https://doi.org/10.1103/PhysRevA.77.012712)

PACS number(s): 03.75.Kk, 03.75.Lm, 05.10.Gg

## I. INTRODUCTION

Since the realization of dilute-gas Bose-Einstein condensates (BECs) [1–3] there have been many experiments on BECs in one-dimensional (1D) optical lattices [4–20]. Neutral atoms in periodic potentials demonstrate a wide range of phenomena that are familiar from other physical systems. Dilute gas BECs are attractive systems in which to study these effects due to the flexibility and control of the experimental apparatus, combined with the existence of microscopic theories that are computationally tractable with various degrees of approximation.

At the simplest level, atoms in an optical lattice are described by Bloch waves familiar from the description of electrons in crystalline condensed matter systems. At sufficiently large densities the interatomic interactions result in a rich range of nonlinear phenomena. Notably, the quantum phase transition from a superfluid to a Mott insulator [5,21] and generation of bright gap solitons [12] have been observed. When the condensate is moving relative to the lattice, the nonlinearity can induce a dynamical (or modulational) instability that leads to an observed heating of the condensate [13–20].

There has been a large amount of theoretical work devoted to instabilities in optical lattices [19,20,22–40]. A stationary solution of the Gross-Pitaevskii equation is susceptible to two types of instabilities: dynamical and energetic. Energetic (or Landau) instabilities exist when the superfluid or condensate is not at a local minimum of energy, and can deplete the condensate via dissipative processes such as interactions with a thermal cloud [32,33]. Dynamical instabilities manifest as an exponential growth of certain modes and are related to the process of parametric amplification. A dynamical instability will rapidly deplete even a pure, isolated condensate. This process will often be chaotic and cause pe-

riod doubling [28,41], turbulence and vortex formation [27], and a loss of coherence of the condensate. A dynamically unstable BEC will eventually thermalize to a higher temperature.

On the other hand, the parametric amplification that causes the dynamical instability can be used to generate interesting states of the condensate. Hilligsøe and Mølmer [42,43] have shown that momentum and energy can be conserved in nontrivial collisions between atoms in a 1D system with a periodic potential. This is in contrast to free space, where such collisions are energetically forbidden. This process is analogous to phase matching in optical parametric amplification, and has been observed with a Bose-Einstein condensate both spontaneously and with seeding by Campbell *et al.* [44]. Related parametric amplification processes have been observed in systems with modulated lattices [41]. Parametric generation creates sub-Poissonian number correlations and quadrature entanglement between different modes in optical experiments, and is expected to do the same for atomic systems [45].

To quantitatively simulate the evolution of dynamical instabilities in a BEC it is necessary to use beyond-mean-field methods for quantum dynamics. In this paper we will be making use of the truncated Wigner method [46–48] that has previously been successfully applied to condensates in optical lattices by a number of authors. First, Polkovnikov and Wang studied the unstable dynamics of an condensate offset in a combined optical lattice plus harmonic potential [34], which lead to dampened Bloch oscillations. Isella and Ruostekoski investigated the dynamics of a trapped condensate as an optical lattice was switched on and found number squeezing in experiments is limited because adiabatic ramping takes a very long time [49,50]. In another work the same authors found that quantum fluctuations cause dissipation via the dynamical instability in the system [35]. Katz *et al.* in-

investigated scattering due to the dynamical instability at the band edge of an optical lattice using a 2D model [20]. They observe that the structure of the scattering halo can deviate strongly from the  $s$ -wave halo in free space.

In this paper we report on experiments where we observe rapid heating of a Bose-Einstein condensate at the band edge of a one-dimensional optical lattice. We identify this heating with the dynamical instability known to be present in this system. We then employ the truncated Wigner method to simulate beyond mean-field quantum dynamics of the system starting from a coherent condensate at zero temperature. We perform a study of the effect of spontaneous processes and dimensionality of the system on the dynamics. In our simulations, we observe dynamical instabilities that lead to heating in qualitative agreement with the experimental results. We attempt quantitative modeling of the experiments and compare our numerical results to the experimental data.

This paper is organized as follows. In Sec. II we describe our experiments where a BEC is loaded into a 1D optical lattice and our observations of the resulting dynamics. We present a theoretical study of the dynamical instability in systems of different dimensionality in Sec. III, highlighting the relative effects of spontaneous and parametric processes. In Sec. IV we present the numerical modeling of the experiment in the nonlinear regime, before concluding in Sec. V.

## II. EXPERIMENTAL RESULTS

### A. Experimental setup

Our experimental setup has previously been described by Mellish *et al.* [11]. Briefly, we use a double magnetic-optical trap setup to collect and pre-cool  $^{87}\text{Rb}$  atoms. The sample is then loaded into a QUIC magnetic trap, from which evaporative cooling results in a Bose-Einstein condensate of approximately  $1 \times 10^5$  atoms in the  $|F=2, m_F=2\rangle$  hyperfine ground state with a condensate fraction of approximately 80%. The peak density in the magnetic trap is  $\sim 1.7 \times 10^{20} \text{ m}^{-3}$  with an axial trap angular frequency of  $\omega_x \approx 2\pi \times 14.6 \text{ Hz}$  and a radial angular frequency of  $\omega_y = \omega_z \approx 2\pi \times 179 \text{ Hz}$ .

In our experiments a weak moving optical lattice is suddenly applied to the condensate at an angle of  $63 \pm 3^\circ$  to the weak axis of the trap. The lattice potential is generated from a single laser of wavelength 780 nm detuned 4.49 GHz from atomic resonance to minimize spontaneous emission. In the lab frame, the two lasers of wave number  $|\mathbf{k}_L| = k_L \approx 2\pi/(780 \text{ nm})$  and angular frequency difference  $\delta$  produce a moving sinusoidal potential

$$V_L(\mathbf{r}, t) = \frac{V_0}{2} \cos(2\mathbf{k}_L \cdot \mathbf{r} - \delta t), \quad (1)$$

where  $V_0$  depends on the intensity of the lasers and the interaction with the atoms. For ease of analysis we define

$$V_0 = s \frac{\hbar^2 k_L^2}{2m}, \quad (2)$$

where  $m$  is the mass of the atoms and  $s$  is a dimensionless quantity that characterizes the depth of the lattice. The fre-

quency difference between the beams is chosen so that relative to the lattice the atoms are moving with a quasimomentum corresponding to the Brillouin zone edge (the Bragg condition). In the frame of the lattice, the atoms are moving with momentum  $-\hbar\mathbf{k}_L$ .

By applying the lattice for an appropriate amount of time one can transfer any fraction of the condensate from one momentum state to the other (Bragg scattering). Alternatively, by phase shifting the optical lattice at the appropriate time one can nonadiabatically load a weakly interacting condensate into an eigenstate of the lattice at either of the lowest two band edges, as described previously in Mellish *et al.* [11].

### B. Experiments in the collisionless regime

We present two sets of experiments in this paper. In the first, after creating the condensate we turn off the magnetic trap and allow the condensate to expand for 10 ms in order to reduce the effect of interactions. This allows for the dissipation of essentially all of the mean-field interaction energy. We then suddenly turn on and hold the optical lattice potential for a total time  $t$ , followed by a further 13 ms expansion (totaling 23 ms since being released from the trap) before imaging. In the frame of the lattice, the condensate begins with momentum  $-\hbar k_L$ , and as expected we find that the condensate undergoes Rabi oscillations between  $\pm \hbar k_L$  momentum.

An absorption image after a lattice evolution time of  $t = 280 \mu\text{s}$  is provided in Fig. 1(a), where we see roughly equal populations in the two momentum modes. To find the populations in each mode, we perform a bimodal fit to the data at momentum  $+\hbar k_0$  and  $-\hbar k_0$ . In the region surrounding each momentum state we fit a Gaussian distribution for the thermal component and an inverted parabola for the condensate. We denote the condensed population in the region of interest surrounding the original condensate as  $N_1$  and that in the second region as  $N_2$ . Similarly we define the total population (condensed and noncondensed) in each region as  $P_1$  and  $P_2$ .

The oscillation between the momentum states is plotted in Fig. 2. From the frequency of this Rabi oscillation ( $5.9 \pm 0.6 \text{ kHz}$ ) we estimate the strength of our optical lattice, and find that  $s \approx 3.1 \pm 0.3$ . The Rabi oscillation is damped due to dephasing caused by the finite momentum width of the wave function of the initial condensate. An exponentially decaying sinusoid is fitted to the data in Fig. 2 for which the damping time is  $400 \pm 200 \mu\text{s}$ .

This experiment can be modeled accurately by mean-field theory. The time-dependent Gross-Pitaevskii equation (GPE) for the evolution of the macroscopic wave function  $\psi(\mathbf{r}, t)$  of a BEC is

$$i\hbar \frac{\partial \psi(\mathbf{r})}{\partial t} = -\frac{\hbar^2}{2m} \nabla^2 \psi(\mathbf{r}) + V(\mathbf{r})\psi(\mathbf{r}) + U_0 |\psi(\mathbf{r})|^2 \psi(\mathbf{r}). \quad (3)$$

The characteristic strength of atomic interactions is  $U_0 = 4\pi\hbar^2 a_s/m$ , where  $a_s$  is the  $s$ -wave scattering length which for  $^{87}\text{Rb}$  we take to be  $a_s = 5.29 \text{ nm}$ . The external potential

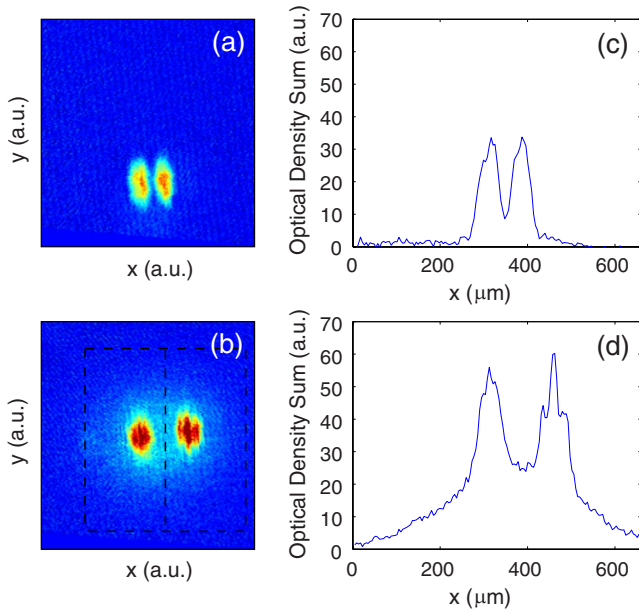


FIG. 1. (Color online) Typical time-of-flight images of a condensate after it has been in an optical lattice at the Brillouin zone boundary (Rabi cycling). Atomic clouds to the right are the atoms that have been Bragg scattered (excited). (a) Collisionless regime  $t=280 \mu\text{s}$  (applied to freely expanding atoms 10 ms after being released from the trap), after 23 ms total time of flight. (b) Nonlinear regime  $t=240 \mu\text{s}$  (applied to trapped atoms) and 29 ms time of flight. The dashed boxes show typical regions of interest used for fitting the data. Also, the clouds in (b) are further apart and larger than those in (a) due to an additional 16 ms of expansion after the lattice is removed. (c) and (d) are  $x$ -axis profiles of the absorption images (a) and (b), respectively, summed along the vertical axis.

$V(\mathbf{r}, t)$  in the experiment is the sinusoidal optical potential from Eq. (1).

As the interactions become negligible after the expansion, a simple one-body theory can be applied to this system [taking  $U_0|\psi|^2=0$  in Eq. (3)]. In Appendix A we derive an ana-

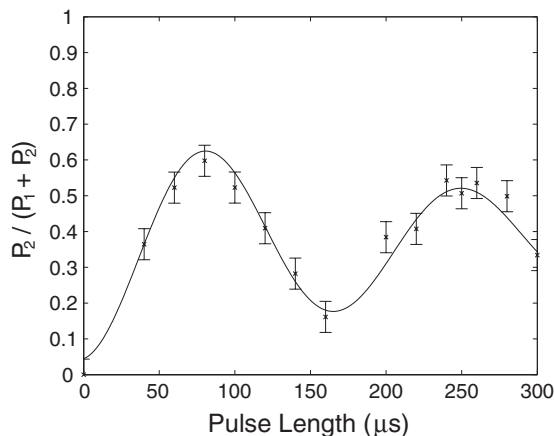


FIG. 2. Fraction of the population that has momentum greater than zero in frame of the lattice (i.e., the Bragg scattered atoms) as a function of the time the lattice is applied after 10 ms of free expansion to reduce the effects of atomic interactions. The solid line is an exponentially decaying sinusoid with a damping time of  $\tau_p = 400 \pm 200 \mu\text{s}$ .

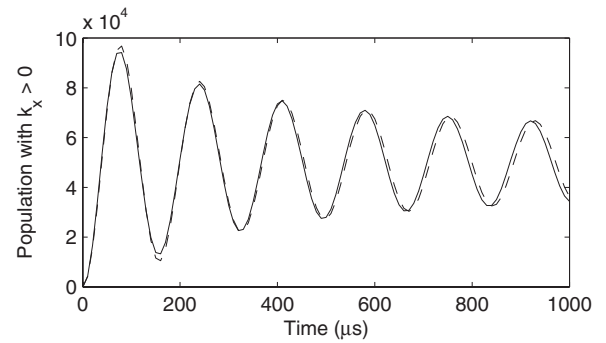


FIG. 3. Comparison of our analytic estimate (4) for the damped Rabi oscillations due to dephasing of a noninteracting condensate (solid line) with a full numerical solution of the Gross-Pitaevskii equation.

lytic expression for the decay based on several approximations. By assuming the initial distribution in momentum space is Gaussian and that the variance of the momentum in the lattice direction,  $\sigma_k^2$ , is due to the kinetic energy released in the expansion we derive the number of scattered atoms as a function of time:

$$N^{(-)} = N_0^{(-)} \left( 1 - \frac{\cos[\omega_0 t + \arctan(t/\tau)/2]}{(1 + t^2/\tau^2)^{1/4}} \right), \quad (4)$$

where  $\tau = sm/16\hbar\sigma_k^2 \approx 174 \mu\text{s}$ . Note that the functional form of this decay is much slower than exponential, and goes as  $t^{-1/2}$  for  $t \gg \tau$ .

To give an idea of the validity of the approximations used to obtain Eq. (4), we also performed a numerical simulation of the condensate expansion followed by application of the optical lattice using the Gross-Pitaevskii equation. Our simulation begins with  $10^5$  atoms in the ground state of the harmonic trap generated by imaginary-time evolution, which has a peak density of  $n_0 \approx 1.69 \times 10^{20} \text{ m}^{-3}$ , followed by a 10 ms expansion. We find that approximately 99.5% of the interaction energy has been converted to kinetic energy after this expansion, so we assume interactions can be safely ignored from this point onwards. We then apply the optical lattice at a  $63^\circ$  angle to the weak trapping axis. By ignoring the nonlinearities in the Bragg process, we dramatically decrease the computational demands of the problem. The number of atoms found to be scattered by the optical lattice by both methods is plotted in Fig. 3, where we find good agreement.

To compare with the experiment, we fitted an exponential decaying sinusoid to the first 300  $\mu\text{s}$  of data in Fig. 3, yielding a decay time of 505  $\mu\text{s}$ , in good agreement with the measured time of  $400 \pm 200 \mu\text{s}$ .

### C. Experiments in the nonlinear regime

In the second set of experiments the optical lattice is suddenly turned on while the condensate is still confined in the magnetic potential. The BEC evolves in the combined potential for a time  $t$  before the lattice, and then the magnetic trap, are both rapidly switched off. An absorption image is then taken after 29 ms of free expansion to observe the resulting

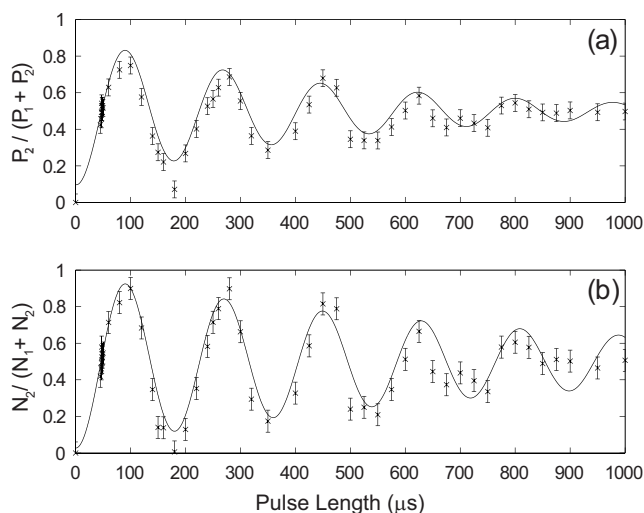


FIG. 4. Bragg scattering experiments performed in the magnetic trap. (a) Fraction of the total population with positive momentum in the frame of the optical lattice as a function of the time. The solid curve is a exponentially decaying sinusoid with a damping time of  $\tau_P = 450 \pm 80 \mu\text{s}$ . (b) Fraction of condensate atoms with positive momentum in trap in the frame of the optical lattice as a function of time. The condensate number is found by fitting a bimodal distribution to each of the condensate peaks as shown in Fig. 1(b). The solid curve is a exponentially decaying sinusoid with a damping time of  $\tau_N = 800 \pm 100 \mu\text{s}$ .

momentum distribution. For the short range of times  $t$  in these experiments there is essentially no change in the atomic density during the evolution in the trap, however, as can be seen in Fig. 1 the momentum distribution undergoes significant evolution. The broad momentum distribution indicates that atoms have been scattered to a variety of different momentum states. The major difference between these experiments and those described in Sec. II B is that the density is much greater while the optical lattice is applied, suggesting that this effect is caused by nonlinear processes.

We observe that a fraction of the atoms still undergo Rabi oscillations between the  $\pm \hbar k_L$  momentum modes. In Fig. 4 we plot the oscillating populations of both the entire sample, and the condensed modes found by the bimodal fitting procedure, finding qualitative agreement with previous results in Ref. [19]. By fitting an exponentially decaying sinusoid, we observe a damping time of  $\tau_P = 450 \pm 80 \mu\text{s}$  for the entire sample. However, we find that the condensed modes oscillate for much longer with a damping time of  $\tau_N = 800 \pm 100 \mu\text{s}$ . It seems reasonable that the damping of the remaining condensate is caused by a similar dephasing mechanism to that of the collisionless regime. The fact that this is longer than the damping time measured in the experiments in the collisionless regime is due to the reduced momentum width of the condensate inside the trap. In the expansion process the interaction energy of the condensate is converted to kinetic energy, resulting in a broader momentum distribution, and therefore faster dephasing. The observed thermal cloud is caused by a distinct nonlinear process. The fraction of noncondensed atoms as a function of the evolution time in the lattice is plotted in Fig. 5. One can see that the noncondensed

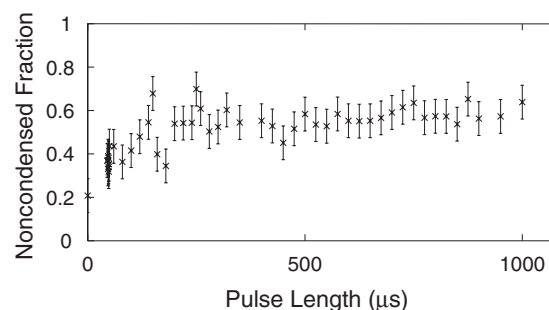


FIG. 5. The noncondensed fraction as a function of time for the Bragg scattering experiments performed in the magnetic trap. The atoms are loaded into the lowest band-edge Bloch state.

fraction grows rapidly until it saturates at about 60%.

We identify the process of heating as due to the dynamical instability of the condensate at the band edge of the optical lattice. If we can assume that the mechanisms of dephasing and instability independently contribute to the exponential damping of the momentum oscillations, we can estimate the total damping time as  $\tau_P^{-1} = \tau_N^{-1} + \tau_{\text{instability}}^{-1}$ . We can then estimate the damping time due to the instability alone to be  $\tau_{\text{instability}} = 1.0_{-0.4}^{+1.2}$  ms. Understanding the heating and damping due to the dynamical instability is the main goal of this paper.

If the processes of dephasing and damping due to heating are truly independent, then we should be able to reproduce the damping time of the oscillations of the condensate fraction as shown in Fig. 4(b) using the 3D Gross-Pitaevskii equation, and we simulate the  $T=0$  condensate dynamics in the combined magnetic and optical potential to test this hypothesis. In Fig. 6 we plot the momentum column density after the lattice is applied to the trapped atoms for (a) 0.5 ms and (b) 1 ms, respectively. The broad, thermal features observed in the experiment are not apparent. However, small ripples in

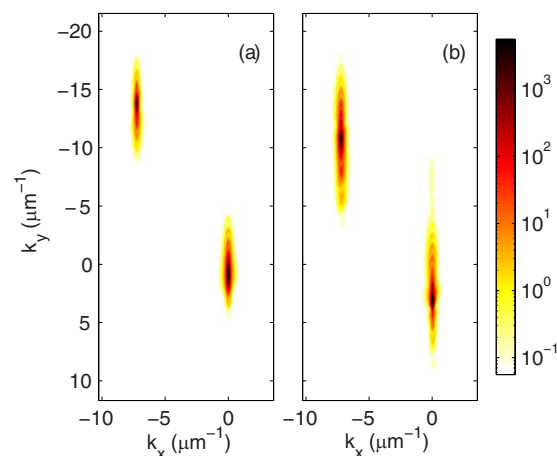


FIG. 6. (Color online) The momentum space column density predicted by a 3D GPE simulation of a trapped BEC after the optical lattice has been applied for (a) 0.5 ms and (b) 1 ms. The  $x$  axis is the weak trapping axis. The condensate is visible about zero momentum and  $2\hbar k_0$ , but no thermal features are visible. Note the “camera” angle is different to the experiment and a logarithmic density scale is used.

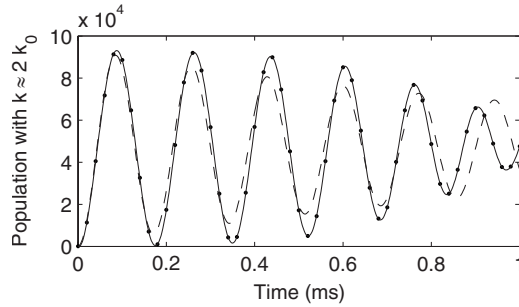


FIG. 7. Total population with positive momentum in the lattice frame for a full 3D GPE calculation corresponding to the in trap experiment showing damped Rabi oscillations. A cubic spline (solid line, to guide the eye) and an exponential decay (dashed line) were fitted to the simulation results (points). The exponential decay constant is  $\tau=1.3$  ms.

the condensate momentum densities are indications of linear dephasing. We observe that the momentum distribution of the condensate modes broadens slowly in time. The center of mass of the two condensates also evolves in time as the condensates climb the walls of the trapping potential. In Fig. 7 we plot the population of the scattered condensate. An exponentially decaying sinusoidal fitted using the least-squares method results in a decay time of 1.3 ms, significantly longer than the experimental measurement of  $\tau_N = 800 \pm 100 \mu\text{s}$ . We note that the exponential decay fits poorly to the numerical results, and that the fitted decay time hence not very well defined.

A similar comparison to an experiment was performed by Katz *et al.* [19], where the authors also observed that GPE simulations did not result in any heating, but did describe dephasing. They found that the GPE predicted a damping rate that, although within experimental error bars, was consistently half as fast as the best-fit damping rate of the experimental data. This is a similar result to what we find here. We therefore conclude that damping of the condensate oscillations is not entirely independent of the dynamical instability leading to the scattering of the condensate atoms and the generation of a thermal cloud.

### III. THEORETICAL STUDY OF DYNAMICAL INSTABILITIES

The character of the dynamical instability in a lattice is dependent on factors including the interaction strength, the number of particles, the strength of the lattice and the dimensionality of the system. The role of excitations in the directions transverse to the lattice was studied thoroughly by Modugno *et al.* [30] who showed that, for small enough  $s$ , there was a significant difference in the stability diagram for 1D and 3D models. In our system, where  $s \approx 3.1$ , we would expect transverse excitations to be an important feature of the dynamical instability.

Although the presence of dynamical instabilities can be found by linearizing the Gross-Pitaevskii equation in the Bogoliubov approach, it cannot accurately describe the dynamics that occurs in an unstable condensate. This is because the

GPE only describes stimulated scattering processes, and for an initial state at zero temperature the quasiparticle modes are unoccupied—the exponential growth expected due to the dynamical instability does not occur as there is no initial seed. However, at zero temperature spontaneous scattering can result in the occupation of quasiparticle modes, seeding the exponential growth and therefore determining the subsequent dynamics of the condensate.

In order to simulate the evolution of dynamically unstable condensates we need to go beyond mean-field theory and implement a method for quantum dynamics that can describe these spontaneous scattering events. This can be achieved with the truncated Wigner method. We find that spontaneous processes initiate parametric growth due to the dynamical instability in the 1D and 2D systems. In three dimensions the spontaneous processes themselves can rapidly deplete the condensate even without parametric amplification as discussed in Sec. III D.

#### A. Quantum model

The second-quantized Hamiltonian for an ultracold Bose gas is

$$\hat{H} = \int d^3\mathbf{r} \left[ \hat{\psi}^\dagger(\mathbf{r}) \left( -\frac{\hbar^2}{2m} \nabla^2 + V(\mathbf{r}, t) \right) \hat{\psi}(\mathbf{r}) + \frac{U_0}{2} \hat{\psi}^\dagger(\mathbf{r}) \hat{\psi}^\dagger(\mathbf{r}) \hat{\psi}(\mathbf{r}) \hat{\psi}(\mathbf{r}) \right], \quad (5)$$

where the field operator  $\hat{\psi}(\mathbf{r})$  annihilates an atom of mass  $m$  at position  $\mathbf{r}$  and obeys the commutation relation  $[\hat{\psi}(\mathbf{r}), \hat{\psi}^\dagger(\mathbf{r}')] = \delta^3(\mathbf{r} - \mathbf{r}')$ .

It is not possible to analytically solve for the evolution of a Bose gas system directly from the Hamiltonian in Eq. (5). Analytical approaches always involve approximations, and often linearize the quantum fluctuations about the mean field as is done in the Bogoliubov approach. Numerical solutions are possible with the exact positive- $\mathcal{P}$  method, but quickly become intractable with sampling problems in many situations [46]. The approximate Gross-Pitaevskii equation (GPE) is straightforward to solve, but fails to account for any spontaneous effects that are important for the problem we are considering.

In this paper we implement the truncated Wigner phase-space method for the system dynamics. This is an approximate method that goes beyond the GPE by including both spontaneous processes and the dynamics of noncondensate modes.

#### 1. The truncated Wigner method

The truncated Wigner method is a phase-space method that approximately solves the dynamics of the Wigner function for the system stochastically. For a system with  $n$  modes the Wigner function is  $2n$  dimensional and it is impractical to solve for directly. However, truncating the third-order derivatives in the equation of motion for the Wigner function results in a Fokker-Planck equation, which can then be simulated using stochastic methods [47,51]. The truncated Wigner

method was used in the context of squeezing of solitons in optical fibres by Carter and Drummond [52], and was first applied to atomic Bose gases by Steel *et al.* [46].

For the Hamiltonian (5) the truncated Wigner method gives a deterministic equation of motion, which happens to be identical to the GPE [Eq. (3)]. The initial conditions, however, are sampled stochastically from the Wigner distribution. Due to the nonzero width of vacuum modes in the Wigner distribution, each unoccupied mode begins with uncorrelated Gaussian noise, normalized to an average of half a particle per mode. This provides the seeding needed for the equation of motion (the GPE) to allow scattering events into these modes, but is subtracted out of all quantum averages. For more details on the truncated Wigner and other phase space methods see Refs. [46–48].

The disadvantage of the truncated Wigner method is that the accuracy of its fundamental approximation is difficult to quantify. However, some work has been done which demonstrates its validity regimes [53,54]. Some of these works have concluded that the major requirement for accuracy is that the number of modes must be much smaller than the number of real particles [55,56], which is the regime we work in for this paper. If this is not the case, then the “vacuum noise” in the initial condition can no longer be considered a perturbation. The vacuum fluctuations will begin to interact as if they are real particles, and unrealistic effects such as negative expectation value for population become prolific [56].

## 2. Simulation parameters

To study the role of spontaneous processes and the effect of dimensionality on the nature of the dynamical instability we chose to implement what we will refer to in this paper as a homogeneous model (strictly a translationally invariant model, where we include the periodic lattice potential but neglect the harmonic trapping potential) with periodic boundary conditions, where the condensate begins with well defined momentum. The spread in momentum found in trapped condensates primarily causes the well understood dephasing effect studied in Sec. II B.

In the experiment the initial inhomogeneous condensate wave function spreads over about 27 wells of optical lattice potential. We use a total population of  $10^5$  atoms and choose to use a density of  $n_0=10^{20} \text{ m}^{-3}$ , roughly corresponding to the average density within the trap rather than the peak density. We have implemented a rectangular grid with periodic boundary conditions for our simulation space, with dimensions  $L_x \times L_y \times L_z$ . The lattice is parallel to the long axis of the space, with spacing 390 nm, extending over 32 wells, making  $L_x=12.48 \mu\text{m}$ . It follows that  $L_y=L_z \approx 8.95 \mu\text{m}$ . Note that this geometry is slightly different to that of the extended condensate at a  $63^\circ$  angle to the lattice.

We begin with a homogeneous cloud moving at the Bragg condition with momentum of  $\hbar k_L$  in the direction of the stationary lattice. The nonlinearity and strength of the lattice are the same as used previously. Care was taken to ensure numerical accuracy, and a projection operator that prevents numerical aliasing [57–59] was employed.

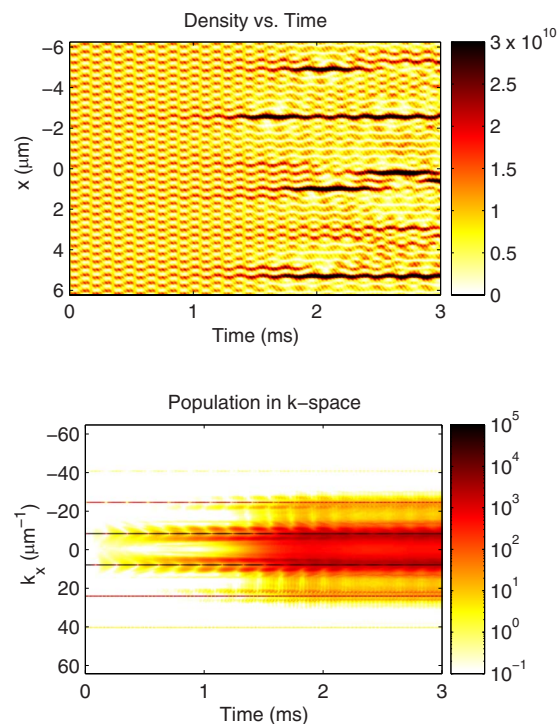


FIG. 8. (Color online) Top: Density (in  $\text{m}^{-1}$ ) of a 1D BEC moving in an optical lattice. We see spontaneous symmetry breaking of the BEC in a single trajectory simulation. The localized regions of high density are bright-gap solitons. Bottom: The same results are presented in momentum space, where symmetry breaking is characterized by mixing into a variety of different modes (note the logarithmic dependence of the density scale).

## B. One dimension

For quasi-one-dimensional systems we can expect a narrow band of modes for which collisions are both resonant (i.e., conserve energy) and conserve momentum modulo  $2\hbar k_L$  (i.e., quasimomentum in the lattice). These are the modes which will undergo rapid exponential growth. At later times, secondary collisions between atoms will lead to thermalization of the system.

Figure 8 shows results for a single trajectory, which in some sense can be considered to be analogous to what might be observed in a single experiment in the lab [53]. In real space we observe spontaneous breaking of the translational symmetry of the lattice brought about by the dynamical instability. The high-density features correspond to generation of bright-gap solitons. These solitons are known to be generated from states near the top of the ground band for condensates with repulsive interactions [23]. The momentum distribution broadens indicating spontaneous collisions between condensate atoms scattering atoms to other momentum modes.

The work of Hilligsøe and Mølmer [42,43] predicts that collisions that conserve energy and momentum (i.e., resonant collisions in the eigenbasis of the lattice) will experience parametric growth. The result of this parametric growth is evident in Fig. 9 where the condensate component stays approximately constant until after one millisecond where depletion begins suddenly. The exponential growth takes some time to become significant.

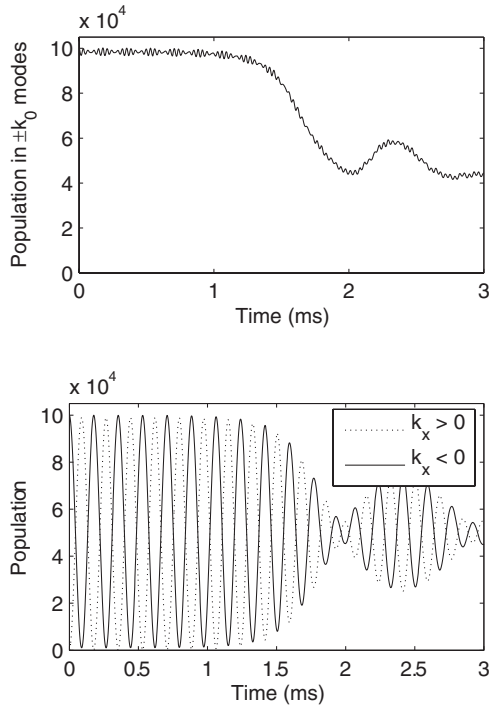


FIG. 9. Top: Sum of the population in the momentum modes  $\pm k_L$  of a 1D Bose gas plotted versus time. The small, rapid oscillations are due to the initial state mixing with higher band states in the Bloch basis. The atoms are depleted from the condensate mode, until a partial revival begins at  $\sim 2$  ms. This is due to Rabi oscillations of the not-quite resonant collisions. Bottom: Total populations of atoms with positive or negative momentum versus time. Damping of the Rabi oscillations is observed in the 1D simulations after 1.5 ms, but then revive at the same time as the condensate as shown in the top figure. Both plots have used an ensemble of 1000 trajectories.

Energy conservation is not quite satisfied for any single mode for all times, and so Rabi oscillations are expected that will hinder the exponential growth of parametric amplification. This is demonstrated in Fig. 9, where population revival into the states  $\pm k_L$  can be seen. Also note that only about half the population is depleted from the two condensate modes—this corresponds to the half that are in the lowest band near the band-edge that generate a bright-gap soliton [23,60].

In this simulation, the condensate begins with well defined momentum and is therefore not subject to linear dephasing as discussed in Sec. II B. However, we observe that oscillations of the condensate component (i.e., the atoms with precisely momentum  $\pm \hbar k_L$ ) are damped as the lower band-edge state is quickly depleted. In Sec. II C we found that the GPE dynamics could not adequately account for the damping of the condensate component. The preferential depletion observed here could potentially explain the discrepancy.

The experiments described in this paper indicate damping of the Rabi oscillations is partially due to dynamical instability. Ensemble averages of 1000 trajectories show damping occurring after a few milliseconds (see Fig. 9) and the approach towards thermal equilibrium. We note that the phase

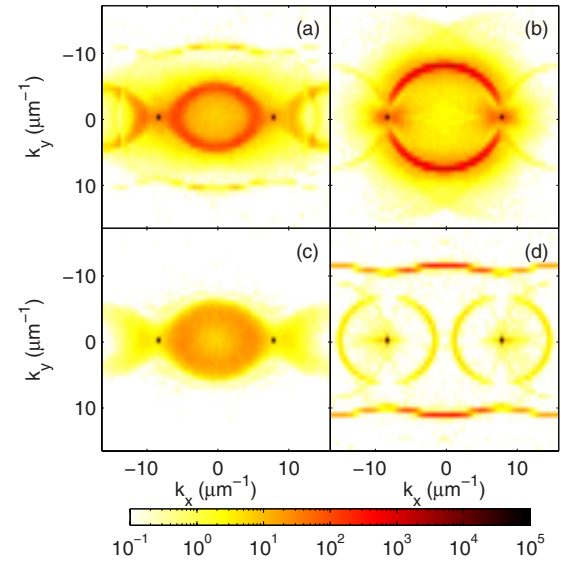


FIG. 10. (Color online) Populations in momentum space of a 2D simulation. The condensate began in (a) the lattice in the  $-k_L$  momentum state,  $t=1.1$  ms. (b) A superposition of  $\pm k_L$  momentum in free-space for comparison with (a),  $t=1.1$  ms. (c) The lowest band-edge of the lattice,  $t=0.36$  ms. (d) The edge of the first excited band,  $t=1.1$  ms.

coherence is also destroyed by the dynamical instability. This is an interesting example of decoherence under Hamiltonian evolution.

We note that to double-check our earlier assertions regarding the Gross-Pitaevskii equation, we have solved the 1D GPE with identical parameters and do not observe any heating or damping of the condensate oscillations before 7 ms, when the dynamical instability causes numerical errors to quickly render the simulation meaningless.

## C. Two dimensions

### 1. Dynamical instability

The effect of dimensionality on the system varies according to the parameters of the experiment and has been dealt with analytically in detail by Modugno *et al.* [30], where the dynamical instability was studied as an exponential growth of Bogoliubov modes. A complete set of Bogoliubov modes includes excitations in the direction of the lattice (such as would be found in a 1D treatment), excitations in the directions perpendicular to the lattice, and excitations that are mixtures of both. For some parameter regimes, the perpendicular excitations are an important part of the dynamics, and the same is true in our homogeneous treatment.

Figure 10 shows a comparison of momentum distributions for four different initial conditions averaged over  $10^3$  trajectories. In Fig. 10(a) the condensate begins in the  $+k_L$  momentum mode; in Fig. 10(b) we make a comparison to free space collisions (without the optical lattice) between momentum modes  $\pm k_L$ . Figures 10(c) and 10(d) begin with the atoms loaded into the ground and first excited band-edge states, respectively. When the moving lattice is switched on such that the BEC is in the  $+k_L$  momentum state, we see compli-

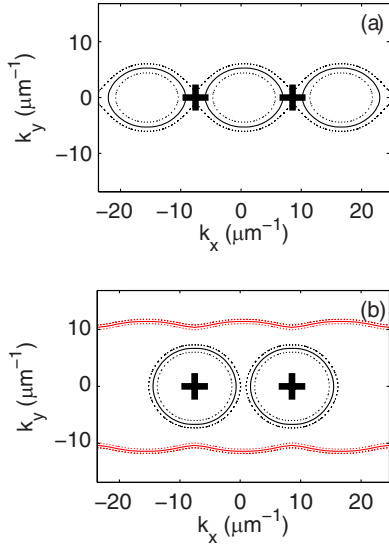


FIG. 11. (Color online) Plots of modes for which the resonance condition is satisfied. The dotted lines correspond to regions close to resonance, having an energy mismatch corresponding to a Rabi oscillation period of 1 ms. The large pluses represent the initial state of the BEC. (a) Two atoms colliding within the lowest band. (b) Two atoms begin in the second band edge can collide to result in an atom in the lowest and second band (inner circles, black online) or two atoms in the lowest band (outer rings, red online).

cated dynamics including Rabi oscillations and scattering into a variety of modes.

We can understand the complicated dynamics by realizing that the initial condition is a superposition of Bloch states at the band edge of the optical lattice [11]. Each of these states has a well-defined energy, and we can analyze which collisions will conserve energy and quasimomentum (modulo  $2k_L$ ) in the Bloch basis. The system has been analyzed previously in a similar fashion [20,43]. Katz *et al.* [20] provided comparisons with the results of truncated Wigner simulations and an experiment. They found, as we do, that the structure of the scattering halo differs significantly from the  $s$ -wave scattering sphere generated by condensate collisions in free space, due to the modified dispersion curve.

Two atoms initially at the edge of the first band can collide to produce atoms elsewhere in that Bloch band, but with additional kinetic energy in the transverse direction. We have calculated the resonance condition using the Hartree-Fock mean-field method [61]. The values of momentum where this occurs is shown in Fig. 11(a) [cf. Fig. 10(c)]. There are two possible outcomes for atoms colliding at the first excited band edge. Either one or both atoms can end up in the lowest band. Both of these cases are presented in Fig. 11(b) [cf. Fig. 10(d)]. Note that the resonance condition is sharper than in Fig 11(a), i.e., there is a smaller total number of modes that have a final energy close to the resonance condition. This explains why there is significantly more scattering in Fig. 10(c) (where the initial condition is in the first band) than in Fig. 10(d) (initial condition in the second band).

## 2. Coherent and incoherent components

We have investigated the phase coherence of the atomic cloud as it undergoes thermalization. A Bose-Einstein con-

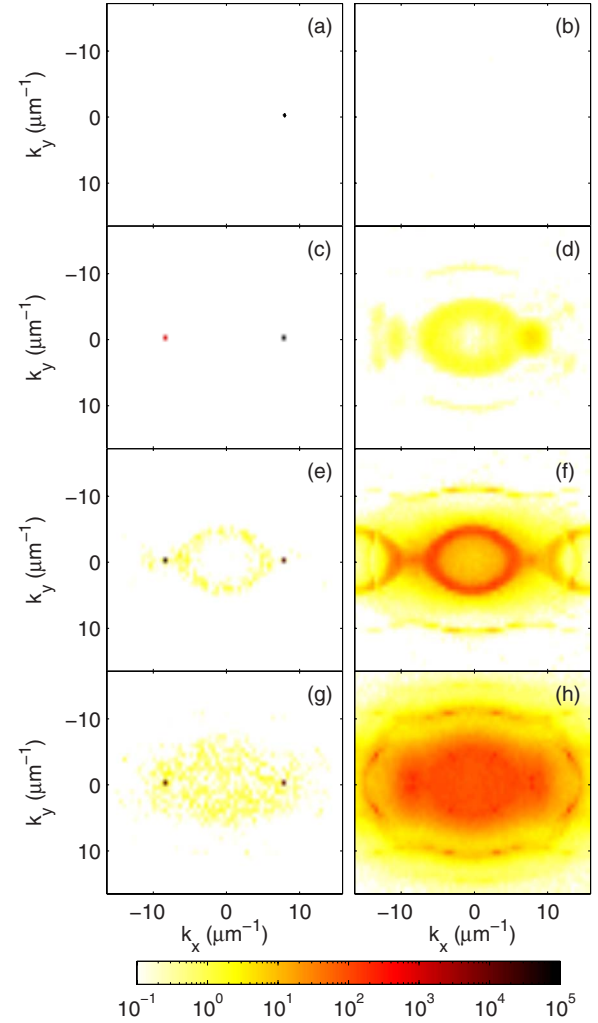


FIG. 12. (Color online) Coherent (a), (c), (e), (g) and incoherent (b), (d), (f), (h) populations in momentum space for the 2D simulation at times 0 (a), (b), 0.56 ms (c), (d), 1.1 ms (e), (f), and 3 ms (g), (h).

densate has off-diagonal, long-range order where there is a well-defined relative phase across the system. When employing classical field methods one typically begins with a coherent state, ascribing a global phase to the condensate at  $t=0$ . If the cloud becomes thermalized then it will lose its phase coherence.

We define the coherent component of the cloud to be that with well-defined global phase

$$N_{\text{coherent}}(\mathbf{k}) = |\langle \hat{a}(\mathbf{k}) \rangle|^2. \quad (6)$$

The incoherent component is the remainder of the atoms

$$N_{\text{incoherent}}(\mathbf{k}) = \langle \hat{a}^\dagger(\mathbf{k}) \hat{a}(\mathbf{k}) \rangle - N_{\text{coherent}}(\mathbf{k}). \quad (7)$$

We plot the coherent and incoherent populations in Fig. 12 for the initial condition with the condensate in momentum state  $|+k_L\rangle$ . Coherent dynamics caused by the lattice drives the condensate into the modes with momentum  $\pm k_L$ ,  $\pm 3k_L$ , etc. Only these modes contain any significant coherent popu-

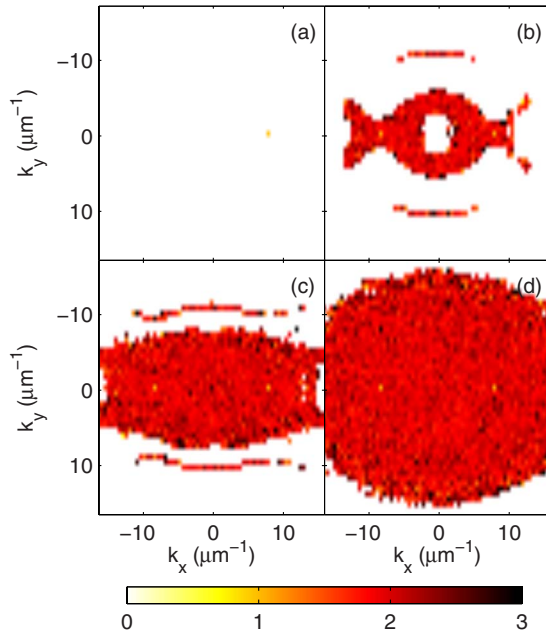


FIG. 13. (Color online) The normalized second-order momentum-space correlation function  $g^{(2)}(\mathbf{k})$  is shown for the 2D simulation at times (a) 0, (b) 0.56, (c) 1.1, and (d) 3.0 ms. Results are only shown for modes with average population greater than  $1/2$ .

lation. Note the noise in Figs. 12(e) and 12(g) is a statistical artifact from averaging over only 1000 trajectories, and could be reduced with more CPU time.

The incoherent population is generated by spontaneous scattering into the noncondensate modes surrounding the condensate. At short times energy conserving collisions from the two condensate modes dominate. At later times further scattering from the newly populated modes broadens the distribution and results in thermalization.

### 3. Local correlation functions

The normalized second-order local momentum-space correlation function is

$$g^{(2)}(\mathbf{k}) = \frac{\langle \hat{a}^\dagger(\mathbf{k}) \hat{a}^\dagger(\mathbf{k}) \hat{a}(\mathbf{k}) \hat{a}(\mathbf{k}) \rangle}{\langle \hat{a}^\dagger(\mathbf{k}) \hat{a}(\mathbf{k}) \rangle^2} \quad (8)$$

and can be calculated using the truncated Wigner method by transforming into symmetric ordering. This correlation function allows us to probe the quantum statistics of each momentum mode—in particular, the occupation statistics in each mode. For coherent, Poissonian statistics  $g^{(2)}=1$ , and for thermal, Gaussian statistics  $g^{(2)}=2$ .

We plot  $g^{(2)}(\mathbf{k}, t)$  in Fig. 13 for the state beginning with momentum  $k_L$ . At all times  $g^{(2)}(\pm k_L) \approx 1$ , and the condensate modes continue to display coherent statistics. However, we see that the all other populated modes have  $g^{(2)} \approx 2$ . These modes are displaying Gaussian statistics which supports the claim that a thermal cloud is growing around the condensate. Comparing Figs. 12 and 13 we see the modes with phase coherence display second-order coherent statistics and those without phase coherence display thermal statistics. Note again that the noise in Fig. 13 is statistical.

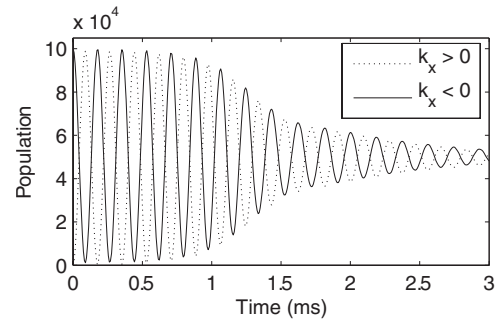


FIG. 14. Time dependence of the total population of all modes with positive or negative momentum in the lattice direction (in the frame of the lattice). These exhibit damped Rabi oscillations in the 2D simulations similar to the 1D results in Fig. 9. Note that onset of damping is more rapid in 2D than 1D, and that revivals are not seen in this case.

### 4. Rabi oscillations

In Fig. 14 we present the time dependence of the population of the positive and negative momentum components for the 2D system. These show damped Rabi oscillations without the revivals that were observed in the 1D simulations. There are many more modes in the 2D system, which has two important effects. First, each mode will Rabi oscillate at a different frequency, and so one expects dephasing to wash out the revival. Second, these modes will interact with each other, and the system will approach thermal equilibrium faster. We also see that the oscillations undergo damping sooner compared to the 1D results. The parametric nature of the process is still evident as it takes some time for the growth of resonant modes to become large enough to significantly affect the Rabi oscillations.

### D. Three dimensions

For higher-dimensional systems there will be a much larger volume in phase space where collisions are close to resonance, most of which incorporate an excitation transverse to the lattice dimension. Due to increased resonant phase-space volume, the total rate of condensate depletion by spontaneous scattering is greatly increased, and correspondingly the effect of Bose enhancement is significantly reduced. For some systems the number in each mode may not grow much at all before the condensate is entirely depleted. In this situation the parametric nature of the dynamical instability will be washed out by spontaneous processes. Note that secondary collisions would also be expected in these systems too, leading to thermalization. Thus, in systems of any dimensionality one could expect to observe rapid thermalization of the condensate.

As an example, consider a system in the limit of a weak lattice (small  $s$ ). In this case the energy spectrum is not modified significantly from the free particle case. However, oscillations in momentum due to the lattice are expected to occur. At the band edge one would expect Rabi oscillations between modes with momentum  $\pm \hbar k_L$ . Assuming that the energy spectrum is not significantly different to free space, one would expect resonant collisions between the modes

with momentum  $\pm\hbar k_L$  into a spherical shell of momentum with modulus  $\hbar k_L$  [53,62,63]. We can derive the spontaneous collision rate using Fermi's second golden rule.

To compare with parameters from our experiment, a system with a total of  $N \approx 10^5$   $^{87}\text{Rb}$  atoms in a volume  $V \approx 10^{-15} \text{ m}^3$  has a spontaneous scattering rate of

$$\frac{dN}{dt} = \frac{U_0^2 N^2 m |k_L|}{2\pi\hbar^3 V} \approx 4 \times 10^7 \text{ s}^{-1}. \quad (9)$$

Thus, 10% of the condensate is lost in just 250  $\mu\text{s}$  by spontaneous collisions. Of course, this value will not be accurate for  $s \approx 3$ , and does not take into account the fact that the atomic populations are oscillating between the two momentum states or the effect of Bose enhancement. This does, however, highlight that rapid heating does not require parametric growth in dynamically unstable 3D systems, but could be simply provided by a sufficiently large density of states at resonance. We present our truncated Wigner simulations in three dimensions in the following section.

#### IV. SIMULATIONS OF THE EXPERIMENT IN THE NONLINEAR REGIME

In this section we numerically model the experiment in the nonlinear regime. Directly modelling the experiment requires a demanding three-dimensional calculation that includes the effects of spontaneous scattering. The truncated Wigner approximation will include spontaneous processes but is known to be inaccurate in some regimes, particularly when the number of particles is less than the number of modes used to simulate them.

Unfortunately, this is the case for the full 3D experimental parameters. Including the trap and the optical lattice while simultaneously avoiding numerical aliasing due to the nonlinearity requires of order  $10^6$  modes to represent  $1 \times 10^5$  atoms. Our attempts at calculations in this regime clearly display unphysical behavior similar to those found in Ref. [56]. In particular, we observe large areas of negative population at high momenta modes, and a corresponding clustering of the vacuum noise at small momentum which swamps the condensate. The condensate is rapidly depleted as it scatters off these unphysical particles.

To proceed we make a further simplification by neglecting the trapping potential, and instead modeling a homogeneous system with similar density to the experiment. By doing so we expect to capture the physics important to the instability, as the timescale over which the heating manifests is much shorter than the trapping periods, so while the optical lattice is on the atoms will essentially be stationary and the density constant. This model requires fewer ( $\sim 4 \times 10^5$ ) modes to simulate the dynamics, and therefore the truncated Wigner method is expected to be more accurate. In Appendix B we perform a basic check of the validity of the truncated Wigner method using the parameters presented here, and find the simulation agrees with known results.

We point out in advance that while our truncated Wigner calculations will model the spontaneous scattering in this system, the homogeneous calculations will not capture the

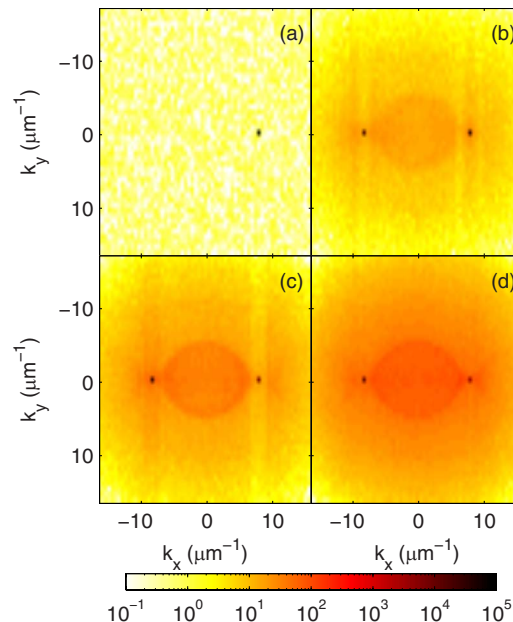


FIG. 15. (Color online) The momentum space column densities for the 3D simulation is shown at times (a) 0, (b) 0.56, (c) 1.1, and (d) 3.0 ms. The scattering halo is clearly visible in (c) and (d).

linear dephasing of the Rabi oscillations in the experiment as the condensate begins in a single momentum state. Instead, we attempt to theoretically predict damping time due to the instability  $\tau_{\text{instability}}$  and compare the value extracted from the experimental data. We also discuss the implications of thermal effects and density, and conclude by estimating a total damping time combining both dephasing and instability mechanisms.

#### A. Truncated Wigner simulation

##### 1. Momentum distribution

In the experiment time-of-flight expansion was used to image the momentum column densities of the system. Figure 15 shows the results of the three-dimensional calculation where we have integrated over the  $z$  momentum component. The ensemble average is for only 32 trajectories due to the computational demands of the simulation. Note that the sharp features seen in the 2D case (Fig. 10) are somewhat washed out, resulting in a distribution more closely resembling two (compact) condensates surrounded by a thermal cloud. However, this is not precisely the case—the population is slightly concentrated in ring-shaped structures in 3D as seen in Fig. 16. These ring-shape structures are similar to those seen in the 2D simulations.

We remind the reader that the simulations performed here are for a homogeneous gas, whereas the trapped condensates in the experiment has a finite momentum width. It seems reasonable to expect that the sharper features would not be as visible in a trapped condensate, and we conclude there is good qualitative agreement between Fig. 15 and the experimental images in Fig. 1 when one takes the effects of the trapping potential into account.

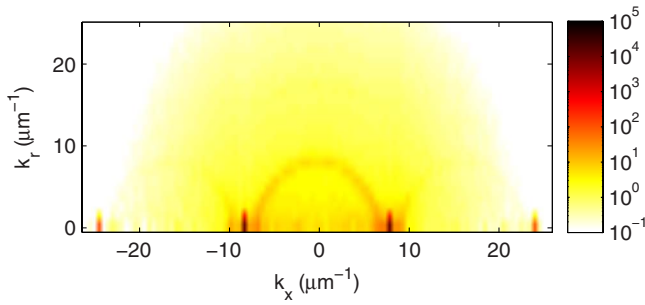


FIG. 16. (Color online) The average population per mode as a function of axial and radial momenta for a 3D simulation at time 3.0 ms.

### 2. Rabi oscillations

We have plotted the total population with a positive component of momentum in the lattice direction in Fig. 17. An exponentially decaying oscillation of the form

$$P_+ = P_0 \cos(\omega t) e^{-t/\tau} \quad (10)$$

was fitted to the data using a least-squares method. The oscillation period was found to be  $2\pi/\omega = 177 \mu\text{s}$ , as expected for a lattice with  $s=3.1$ .

The decay constant was found to be  $\tau=2.00$  ms. This result does not include the effects of linear dephasing and should be compared to the experimentally determined value for  $\tau_{\text{instability}} = 1.0_{-0.4}^{+1.2}$  ms. In the 1D simulations it was noted that the upper and lower band-edge states were depleted at different rates leading to saturation of the thermal component at around 50%. Similarly, in the experiment the condensate oscillations damp faster than predicted by the GPE, and the thermal component saturates at around 60%. However, for the 3D simulations presented here the oscillations of the condensate component (i.e., that with precisely momentum  $\pm \hbar k_L$ ) are not damped in this simulation, and the upper and lower band-edge states are depleted at a similar rate. It is unclear whether this holds for the true trapping geometry which we are unable to simulate, and so we cannot explain the reason behind the discrepancy in the GPE dephasing time and the experimentally determined condensate damping time. As an additional check we have also solved the 3D

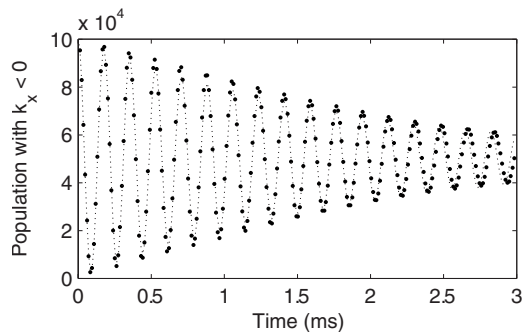


FIG. 17. Population of the momentum modes with  $k_x < 0$  for the 3D simulations. We see damped Rabi oscillations similar to Figs. 9 and 14. A decaying exponential fit (dotted line) has been made with the numerical results (points), with period  $177 \mu\text{s}$  and decay time constant 2.00 ms.

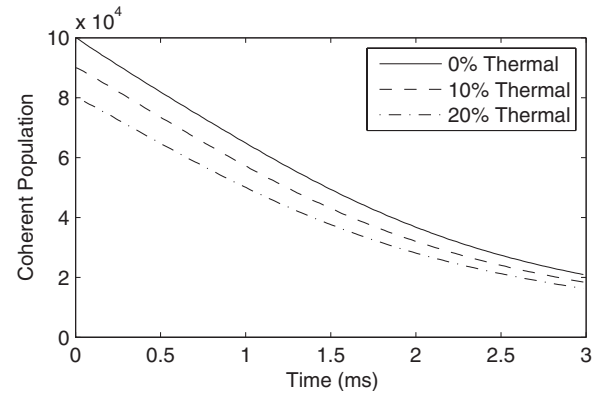


FIG. 18. The total coherent population of the condensate beginning at temperatures corresponding to pure condensate, 90% condensate, and 80% condensate. All simulations contain a total population of  $10^5$  atoms.

GPE with identical parameters for 1 ms of evolution in the optical lattice, and as in the 1D case we do not observe any heating or damping of the condensate oscillations over this time scale.

## B. Temperature and density

The dynamics of this system are quite sensitive to some parameters that are difficult to measure precisely in an experiment, such as atom number, density, and temperature. We will now investigate the effect of finite temperature and higher density.

### 1. Finite temperature

The simulations we have presented so far have all begun with initial states sampled from the zero temperature Wigner distribution for the condensate. However, if the system is in fact at any nonzero temperature then any surrounding thermal cloud is able to increase the rate of depletion by means of Bose enhancement of the resonant collisions. We have performed a 3D simulation with the same parameters as described in Sec. IV A, but with a 10 and 20 % thermal fraction surrounding the pure condensate centered with momentum  $+\hbar k_L$ . Note that the experiments began with approximately a 20% thermal fraction.

In Fig. 18 we plot condensate fractions as a function of time. Fermi's golden rule for scattering predicts that the scattering rate is proportional to the square of the number of condensate atoms [cf. Eq. (9)]. However, such a calculation does not take into account the population of the modes to which atoms are scattered into. A closer look at the results in Fig. 18 indicate that the fractional rate of loss of the coherent component is actually slightly greater in the cases where a thermal cloud is present after a time of  $200 \mu\text{s}$ . The Bose-enhancement due to the thermal fraction outweighs the reduction in condensate fraction.

The oscillations are damped faster at higher temperatures. An oscillating exponential decay yields damping times of  $\tau \approx 2.00, 1.76, \text{ and } 1.61$  ms for 0, 10, and 20 % thermal fraction, respectively. Thus we can conclude that the damping rate is relatively sensitive to the presence of a thermal fraction.

TABLE I. The rates of damping in the simulations and experiments. The combined theory damping time is a combination of the theoretical dephasing time from the 3D GPE (which disagrees with experiment) and damping time from the dynamical instability.

| Description          | Density (m <sup>-3</sup> )    | Thermal fraction | Damping time                           |
|----------------------|-------------------------------|------------------|--|
| Collisionless theory |                               |                  | 505 $\mu$ s                            |
| Collisionless expt.  |                               |                  | 400 $\pm$ 200 $\mu$ s                  |
| GPE in trap          |                               |                  | 1.3 ms                                 |
| Dephasing expt.      |                               |                  | 800 $\pm$ 100 $\mu$ s                  |
| Truncated Wigner     | 1.0 $\times$ 10 <sup>20</sup> | 0%               | 2.00 ms                                |
| Truncated Wigner     | 1.0 $\times$ 10 <sup>20</sup> | 10%              | 1.76 ms                                |
| Truncated Wigner     | 1.0 $\times$ 10 <sup>20</sup> | 20%              | 1.61 ms                                |
| Truncated Wigner     | 1.7 $\times$ 10 <sup>20</sup> | 0%               | 1.22 ms                                |
| Truncated Wigner     | 1.7 $\times$ 10 <sup>20</sup> | 20%              | 1.00 ms                                |
| Instability expt.    |                               | $\sim$ 20%       | 1.0 <sup>+1.2</sup> <sub>-0.4</sub> ms |
| Combined theory      | 1.7 $\times$ 10 <sup>20</sup> | 20%              | 560 $\mu$ s                            |
| Trapped expt.        |                               | $\sim$ 20%       | 450 $\pm$ 80 $\mu$ s                   |

## 2. Peak-density calculation

Until now our choice of density for the calculations has been the approximate average density of the condensate in the experiment. Here we repeat the simulations using instead the peak density of  $1.7 \times 10^{20}$  atoms m<sup>-3</sup>. We have no *a priori* reason to prefer one over the other. However, as the scattering will occur quickest in the region of highest density, one might expect the dynamics in the peak-density region to dominate.

We performed simulations at zero temperature and with a 20% thermal fraction, finding damping rates of 1.22 and 1.00 ms, respectively. This highlights the sensitivity of our results to both our choice of either the peak or average density, and also that experimental error in determining atom number and density has a significant impact on the resulting dynamics.

## C. Dephasing and instability

A summary of the results of all our 3D calculations and the experimental results are shown in Table I. We note that both the average and peak density damping rates give a result compatible with the experimental observations, but that the dephasing in the GPE simulation including the effect of the trap was slower than the observed 800  $\mu$ s.

We can combine the results of the linear dephasing and the simulation of the dynamical instability. In the simplest model for decay of the Rabi oscillations, we would simply add the two exponential decay rates by  $\tau^{-1} = \tau_{\text{dephasing}}^{-1} + \tau_{\text{instability}}^{-1}$ . For example, using the damping time found with the peak density of  $1.7 \times 10^{20}$  m<sup>-3</sup> and a 20% thermal fraction results in a decay constant of  $\tau \approx 560$   $\mu$ s, which is slightly longer than in the experiment.

Given the degree of approximation necessary in separating the dephasing and instability mechanisms theoretically,

and the experimental uncertainty in some parameters, we must assign a rather large uncertainty to this theoretical prediction. However, to our knowledge it is the first such quantitative calculation to-date for a system in this regime, and is in reasonable agreement with the experimental result.

## V. CONCLUSIONS

In summary, we have described experiments demonstrating the interaction-induced instability of a BEC at the band-edge of a 1D optical lattice. We have performed a thorough theoretical study of the effects of dynamical instabilities in one-, two-, and three-dimensional systems, demonstrating different regimes of the dynamical instability. We found that parametric growth is important in lower dimensional systems but that spontaneous scattering dominates the dynamics in 3D. We have attempted to quantitatively model the dynamics of this system by simulating a size-matched homogeneous system using the truncated Wigner method, with reasonable agreement between our experimental and theoretical results for damping due to the dynamical instability.

Our truncated Wigner simulations produced slightly slower scattering and damping of Rabi oscillations than observed in the experiment and showed that the scattering rate is larger for nonzero temperatures. However, in our simulations we have neglected the trapping potential in order to find a regime in which the truncated Wigner technique was accurate. We have included some of the consequences of the trap using mean-field calculations, and estimated their contribution to damping of Rabi oscillations. We find this predicts a significantly longer damping time for the condensate oscillations than observed in experiment, similar to the results of Katz *et al.* [19]. Thus it seems that dephasing cannot be simply separated from the heating from the dynamical instability.

Although the truncated Wigner method has had limitations in the particular experiments presented here, there are many other experiments to which it could be applied. In particular, systems of reduced dimensionality where the condensate is tightly confined in one or two directions (i.e., waveguides) will be well modeled with the truncated Wigner method. This will allow quantitative analysis of nonclassical effects in condensates, such as spontaneous scattering, number squeezing effects, and entanglement between atoms and with light.

## ACKNOWLEDGMENTS

A.J.F. and M.J.D. would like to thank Murray Olsen and Ashton Bradley for useful discussions, and Elena Ostrovskaya for initiating our interest in heating in lattices. This work was funded by the Australian Research Council Centre of Excellence for Quantum-Atom Optics, the Queensland State Government, and the Marsden Fund of New Zealand.

## APPENDIX A: DAMPED OSCILLATIONS IN THE LINEAR REGIME

We derive an analytic approximation to the form of the damped oscillations in the linear regime. The Rabi frequency

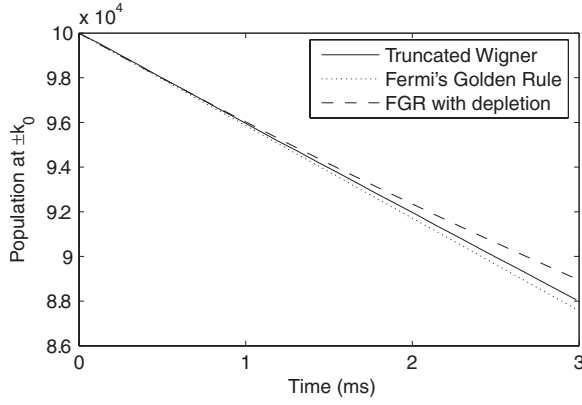


FIG. 19. Condensate occupation of the modes  $\pm\hbar k_L$  versus time for a condensate collision in free space. We compare predictions from truncated Wigner simulations (solid), a straight line fit to the rate given by Fermi's golden rule (dotted), and the solution to the differential equation Eq. (9) that includes condensate depletion (dashed).

of oscillation of an atom is dependent on its initial momentum, and the momentum width of the condensate gives a spread of Rabi frequencies whose sum results in the damping of the full oscillations.

It is worth noting that the dimensionality of the problem can be reduced. Any momentum orthogonal to the lattice does not affect the oscillation frequency, and therefore is not a part of our dephasing analysis. Thus, we only need to look at the distribution of momenta in the lattice direction. We introduce a few approximations below.

To simplify analysis, our initial distribution was taken to be Gaussian

$$P(k) \propto \exp\left(-\frac{(k - k_L)^2}{2\sigma_k^2}\right), \quad (\text{A1})$$

where almost all of our kinetic energy comes from the released interaction energy  $U_{\text{int}} = \frac{2}{7}U_0 n_0$ , where  $n_0$  is the peak density. Due to the high aspect ratio of the trap, almost all this energy is distributed equally in the two tightly trapped dimensions. Given that the lattice is at angle  $\theta \approx 63^\circ$  to the weak axis of the trap, the conservation of energy requires that

$$\frac{\hbar^2 \sigma_k^2}{2m} = \frac{\sin^2 \theta}{7} U_0 n_0. \quad (\text{A2})$$

This results in a predicted  $\sigma_k \approx 1.60 \times 10^6 \text{ m}^{-1}$ .

We will now analyze the dynamics of these modes. In a periodic potential, the eigenstates are superpositions of momentum states corresponding to the same quasimomentum (i.e.,  $\hbar k \pm 2n\hbar k_L$ , where  $n$  is an integer). We can then find the rate of oscillation between two modes of the same quasimomentum. At the band edge, we assume the eigenstates to be superpositions of the momentum modes  $|\pm k_L\rangle$ . The energy difference  $\hbar\omega_0$  between the two states at the band edge

$$\hbar\omega_0 = \frac{\hbar^2 k_L^2 s}{2m}, \quad (\text{A3})$$

is accurate for small values of  $s$ , and has a 1% error (compared to direct diagonalization) for the value of  $s=3.1$  used in these simulations and experiments. The Rabi frequency of the oscillation is  $\omega_0$ .

We now determine how the oscillation frequency varies with the quasimomentum. We will assume that the eigenstates are superpositions of the modes  $|\Delta k + k_L\rangle$  and  $|\Delta k - k_L\rangle$  only. In this basis, we see the energy difference between the upper and lower states is (to second order in  $\Delta k$ ):

$$\hbar\omega \approx \hbar\omega_0 + \frac{8\hbar^2(\Delta k)^2}{sm}. \quad (\text{A4})$$

We can now use this dispersion relation, and the initial conditions of Eq. (A1) to find the distribution as a function of  $\omega$ . Performing the Fourier transform yields the population of the negative momentum modes in time

$$N^{(-)} = N_0^{(-)} \left( 1 - \frac{\cos[\omega_0 t + \arctan(t/\tau)/2]}{(1 + t^2/\tau^2)^{1/4}} \right),$$

where  $\tau = sm/16\hbar\sigma_k^2 \approx 174 \mu\text{s}$ , as plotted in Fig. 3.

## APPENDIX B: ACCURACY OF THE TRUNCATED-WIGNER METHOD

The truncated Wigner method for quantum dynamics is an approximation that is only known to be accurate in certain regimes [53–56,64]. It is known to be accurate under the condition that there are many more particles in the simulation than modes. For the experiment we are considering this is difficult to achieve, as in three dimensions the number of modes can easily be greater than  $10^6$ . Thus, in our calculations we took great care to use the minimum possible number of modes without misrepresenting the physics. To this end we incorporated a projector to implement a spherical cutoff in momentum space at a radius slightly greater than where the atoms can be expected to be found as estimated from lower-dimensional simulations. On the other hand, a sufficiently large grid must be used to eliminate the effects of numerical aliasing [57–59]. This reduces the number of modes to  $\sim 4 \times 10^5$ , for the simulation of  $10^5$  atoms. The truncated Wigner method will not be accurate for long time scales under these conditions, but we are confident that the dynamics we see in relatively short time scales here is accurate.

We have not implemented the method presented by Polkovnikov [54,64] to check the validity of our truncated Wigner simulation. Instead, we have tested our accuracy by comparing the spontaneous scattering rates from a simulation with atoms with momentum  $\pm\hbar k_L$  with Fermi's second golden rule, Eq. (9), for the same parameters used in the other simulations but without the lattice potential. The number of atoms remaining in the  $\pm\hbar k_L$  momentum modes is plotted as a function of time in Fig. 19. At small times the results agree well. We can see the effect of Bose-enhancement at later times when Fermi's golden rule underestimates the depletion rate.

- [1] M. H. Anderson, J. R. Ensher, M. R. Matthews, C. E. Wieman, and E. A. Cornell, *Science* **269**, 198 (1995).
- [2] K. B. Davis, M.-O. Mewes, M. R. Andrews, N. J. van Druten, D. S. Durfee, D. M. Kurn, and W. Ketterle, *Phys. Rev. Lett.* **75**, 3969 (1995).
- [3] C. C. Bradley, C. A. Sackett, J. J. Tollett, and R. G. Hulet, *Phys. Rev. Lett.* **75**, 1687 (1995).
- [4] Y. B. Ovchinnikov, J. H. Müller, M. R. Doery, E. J. D. Vredenbregt, K. Helmerson, S. L. Rolston, and W. D. Phillips, *Phys. Rev. Lett.* **83**, 284 (1999).
- [5] C. Orzel, A. K. Tuchman, M. L. Fenselau, M. Yasuda, and M. A. Kasevich, *Science* **291**, 2386 (2001).
- [6] W. K. Hensinger *et al.*, *Nature (London)* **412**, 52 (2001).
- [7] F. S. Cataliotti, S. Burger, C. Fort, P. Maddaloni, F. Minardi, A. Trombettoni, A. Smerzi, and M. Inguscio, *Science* **293**, 841 (2001).
- [8] M. Greiner, I. Bloch, O. Mandel, T. W. Hänsch, and T. Esslinger, *Appl. Phys. B: Lasers Opt.* **73**, 769 (2001).
- [9] M. Cristiani, O. Morsch, J. H. Müller, D. Ciampini, and E. Arimondo, *Phys. Rev. A* **65**, 063612 (2002).
- [10] J. H. Denschlag, J. E. Simsarian, H. Häffner, C. McKenzie, A. Browaeys, D. Cho, K. Helmerson, S. L. Rolston, and W. D. Phillips, *J. Phys. B* **35**, 3095 (2002).
- [11] A. S. Mellish, G. Duffy, C. McKenzie, R. Geursen, and A. C. Wilson, *Phys. Rev. A* **68**, 051601(R) (2003).
- [12] B. Eiermann, T. Anker, M. Albiez, M. Taglieber, P. Treutlein, K.-P. Marzlin, and M. K. Oberthaler, *Phys. Rev. Lett.* **92**, 230401 (2004).
- [13] S. Burger, F. S. Cataliotti, C. Fort, F. Minardi, M. Inguscio, M. L. Chiofalo, and M. P. Tosi, *Phys. Rev. Lett.* **86**, 4447 (2001); B. Wu and Q. Niu, *Phys. Rev. A* **64**, 061603(R) (2001); B. Wu and Q. Niu, *Phys. Rev. Lett.* **89**, 088901 (2002); S. Burger, F. S. Cataliotti, C. Fort, F. Minardi, M. Inguscio, M. L. Chiofalo, and M. P. Tosi, *ibid.* **89**, 088902 (2002).
- [14] F. S. Cataliotti, L. Fallani, F. Ferlaino, C. Fort, P. Maddaloni, and M. Inguscio, *New J. Phys.* **4**, 71 (2003).
- [15] M. Cristiani, O. Morsch, N. Malossi, M. Jona-Lasinio, M. Anderlini, E. Courtade, and E. Arimondo, *Opt. Express* **12**, 4 (2004).
- [16] L. Fallani, L. De Sarlo, J. E. Lye, M. Modugno, R. Saers, C. Fort, and M. Inguscio, *Phys. Rev. Lett.* **93**, 140406 (2004).
- [17] L. De Sarlo, L. Fallani, J. E. Lye, M. Modugno, R. Saers, C. Fort, and M. Inguscio, *Phys. Rev. A* **72**, 013603 (2005).
- [18] C. D. Fertig, K. M. O'Hara, J. H. Huckans, S. L. Rolston, W. D. Phillips, and J. V. Porto, *Phys. Rev. Lett.* **94**, 120403 (2005).
- [19] N. Katz, R. Ozeri, E. Rowen, E. Gershnel, and N. Davidson, *Phys. Rev. A* **70**, 033615 (2004).
- [20] N. Katz, E. Rowen, R. Ozeri, and N. Davidson, *Phys. Rev. Lett.* **95**, 220403 (2005).
- [21] M. Greiner, O. Mandel, T. Esslinger, T. W. Hänsch, and I. Bloch, *Nature (London)* **415**, 39 (2002).
- [22] F. K. Abdullaev, B. B. Baizakov, S. A. Darmanyan, V. V. Konotop, and M. Salerno, *Phys. Rev. A* **64**, 043606 (2001).
- [23] V. V. Konotop and M. Salerno, *Phys. Rev. A* **65**, 021602(R) (2002).
- [24] B. Wu and Q. Niu, *New J. Phys.* **5**, 104 (2003).
- [25] C. Menotti, A. Smerzi, and A. Trombettoni, *New J. Phys.* **5**, 112 (2003).
- [26] M. Machholm, C. J. Pethick, and H. Smith, *Phys. Rev. A* **67**, 053613 (2003).
- [27] R. G. Scott, A. M. Martin, T. M. Fromhold, S. Bujkiewicz, F. W. Sheard, and M. Leadbeater, *Phys. Rev. Lett.* **90**, 110404 (2003).
- [28] M. Machholm, A. Nicolin, C. J. Pethick, and H. Smith, *Phys. Rev. A* **69**, 043604 (2004).
- [29] Y. Zheng, M. Kostrun, and J. Javanainen, *Phys. Rev. Lett.* **93**, 230401 (2004).
- [30] M. Modugno, C. Tozzo, and F. Dalfovo, *Phys. Rev. A* **70**, 043625 (2004).
- [31] F. Nesi and M. Modugno, *J. Phys. B* **37**, S101 (2004).
- [32] M. Modugno, C. Tozzo, and F. Dalfovo, *Phys. Rev. A* **71**, 019904(E) (2005).
- [33] K. Igaya, S. Konabe, I. Danshita, and T. Nikuni, *Phys. Rev. A* **74**, 053611 (2006).
- [34] A. Polkovnikov and D.-W. Wang, *Phys. Rev. Lett.* **93**, 070401 (2004).
- [35] J. Ruostekoski and L. Isella, *Phys. Rev. Lett.* **95**, 110403 (2005).
- [36] A. Polkovnikov, E. Altman, E. Demler, B. Halperin, and M. D. Lukin, *Phys. Rev. A* **71**, 063613 (2005).
- [37] J. Gea-Banacloche, A. M. Rey, G. Pupillo, C. J. Williams, and C. W. Clark, *Phys. Rev. A* **73**, 013605 (2006).
- [38] A. M. Rey, G. Pupillo, C. W. Clark, and C. J. Williams, *Phys. Rev. A* **72**, 033616 (2005).
- [39] A. V. Ponomarev and A. R. Kolovsky, *Laser Phys.* **16**, 367 (2005).
- [40] E. Altman, A. Polkovnikov, E. Demler, B. I. Halperin, and M. D. Lukin, *Phys. Rev. Lett.* **95**, 020402 (2005).
- [41] N. Gemelke, E. Sarajlic, Y. Bidel, S. Hong, and S. Chu, *Phys. Rev. Lett.* **95**, 170404 (2005).
- [42] K. M. Hilligsøe and K. Mølmer, *Phys. Rev. A* **71**, 041602(R) (2005).
- [43] K. Mølmer, *New J. Phys.* **8**, 170 (2006).
- [44] G. Campbell, J. Mun, M. Boyd, E. Streed, W. Ketterle, and D. Pritchard, *Phys. Rev. Lett.* **96**, 020406 (2006).
- [45] M. K. Olsen and M. J. Davis, *Phys. Rev. A* **73**, 063618 (2006).
- [46] M. J. Steel, M. K. Olsen, L. I. Plimak, P. D. Drummond, S. M. Tan, M. J. Collett, D. F. Walls, and R. Graham, *Phys. Rev. A* **58**, 4824 (1998).
- [47] C. W. Gardiner and P. Zoller, *Quantum Noise*, 2nd ed. (Springer, Berlin, 1999).
- [48] C. W. Gardiner and M. J. Davis, *J. Phys. B* **36**, 4731 (2003).
- [49] L. Isella and J. Ruostekoski, *Phys. Rev. A* **72**, 011601(R) (2005).
- [50] L. Isella and J. Ruostekoski, *Phys. Rev. A* **74**, 063625 (2006).
- [51] C. W. Gardiner, *Handbook of Stochastic Methods*, 2nd ed. (Springer, Berlin, 1985).
- [52] S. J. Carter, P. D. Drummond, M. D. Reid, and R. M. Shelby, *Phys. Rev. Lett.* **58**, 1841 (1987).
- [53] A. A. Norrie, R. J. Ballagh, and C. W. Gardiner, *Phys. Rev. A* **73**, 043617 (2006).
- [54] A. Polkovnikov and V. Gritsev, e-print arXiv:0706.0212.
- [55] A. Sinatra, C. Lobo, and Y. Castin, *J. Phys. B* **35**, 3599 (2002).
- [56] P. Deuar and P. D. Drummond, *Phys. Rev. Lett.* **98**, 120402 (2007).
- [57] M. J. Davis, R. J. Ballagh, and K. Burnett, *J. Phys. B* **34**, 4487 (2001).
- [58] M. J. Davis, S. A. Morgan, and K. Burnett, *Phys. Rev. Lett.* **87**, 160402 (2001).

- [59] M. J. Davis, S. A. Morgan, and K. Burnett, Phys. Rev. A **66**, 053618 (2002).
- [60] B. J. Dabrowska-Wüster, S. Wüster, A. S. Bradley, M. J. Davis, and E. A. Ostrovskaya, e-print arXiv:cond-mat/0607332.
- [61] C. J. Pethick and H. Smith, *Bose-Einstein Condensation in Dilute Gases* (Cambridge University Press, Cambridge, 2001).
- [62] J. M. Vogels, K. Xu, and W. Ketterle, Phys. Rev. Lett. **89**, 020401 (2002).
- [63] A. A. Norrie, R. J. Ballagh, and C. W. Gardiner, Phys. Rev. Lett. **94**, 040401 (2005).
- [64] A. Polkovnikov, Phys. Rev. A **68**, 053604 (2003).